

<https://doi.org/10.1038/s41612-025-01005-z>

# Impacts of abatement in anthropogenic emissions in the context of China's carbon neutrality on global photovoltaic potential

Check for updates

Zhiyao Hu<sup>1</sup>, Zhili Wang<sup>1</sup> ✉, Zhun Guo<sup>2</sup>, Yadong Lei<sup>1</sup> ✉, Xiaochao Yu<sup>1</sup>, Yingfang Li<sup>1</sup>, Lin Liu<sup>1</sup>, Huizheng Che<sup>1</sup> & Xiaoye Zhang<sup>1</sup>

Anthropogenic emission reductions resulting from carbon neutrality and clean air policies in China, one of the world's major emitters of carbon dioxide (CO<sub>2</sub>) and aerosols, are likely to influence regional and global photovoltaic (PV) outputs by affecting climate change. Here, we use the Community Earth System Model version 2 (CESM2) to assess quantitatively how China's emission reductions toward carbon neutrality will influence the PV potential (PV<sub>POT</sub>) and the extremely low PV outputs in the mid-21<sup>st</sup> century (2041–2060). We find that the large reductions in anthropogenic emissions in the context of China's carbon neutrality will increase the PV<sub>POT</sub> and reduce the occurrence of extremely low PV outputs over some regions in the mid-low latitude continents, especially in East Asia, mainly through increasing the downwelling solar flux at the surface. Our results indicate that China's carbon neutrality and clean air policies will not only trigger local positive feedback between anthropogenic emission reductions and PV increases but will also generate additional PV enhancements to remote regions, including eastern Australia, South Asia, southern Africa, and eastern South America. This will ultimately accelerate the process of global carbon neutrality in the coming decades.

The increases in anthropogenic greenhouse gas (GHG) emissions have led to a sustained rise in global mean surface temperature (GMST)<sup>1</sup>. Projections from Earth system models indicate that continued global warming will lead to more frequent and intense extreme weather and climate events<sup>1–3</sup>. To mitigate relevant climate risks, the world nations reached a consensus in Paris to hold the increase in GMST to well below 2 °C and pursue efforts to limit the GMST increase to 1.5 °C above pre-industrial levels<sup>4</sup>. This means that carbon neutrality must be achieved by the mid-to-late 21<sup>st</sup> century, which requires adjustments to the energy mix that is currently dominated by fossil fuels and an acceleration of the transition to a new power system dominated by clean energy<sup>1,5,6</sup>. The deployment of solar photovoltaic (PV), one of the primary sources of clean energy, has avoided global carbon dioxide (CO<sub>2</sub>) emissions of approximately 1.1 Gt per year and plays an important role in the energy transition<sup>7,8</sup>. However, PV outputs are significantly affected by meteorological conditions. For example, cloud cover and aerosol optical depth (AOD) can affect the amount of solar radiation reaching PV panels<sup>9–11</sup>. Temperature and wind speed also impact the efficiency of PV power generation<sup>12–14</sup>. Therefore, PV power generation and its stability are closely related to climate change.

As one of the world's largest emitters of CO<sub>2</sub>, China has pledged to peak its carbon emissions before 2030 and achieve carbon neutrality by 2060. Changes in anthropogenic CO<sub>2</sub> emissions will have a significant impact on future global and regional climate change<sup>15,16</sup>. Recent research<sup>16</sup> has shown that achieving net-zero CO<sub>2</sub> emissions in China could mitigate global warming by 0.16–0.21 °C by the end of the 21<sup>st</sup> century. Simultaneously, the anthropogenic aerosols emitted alongside CO<sub>2</sub> will also be significantly reduced in the future. China's carbon neutrality and clean air policies are predicted to decline the atmospheric concentrations of fine particulate matter (PM<sub>2.5</sub>) in China from 33.4 μg m<sup>-3</sup> in 2020 to 24.6 μg m<sup>-3</sup> in 2030 and 7.6 μg m<sup>-3</sup> in 2060<sup>17</sup>. Changes in anthropogenic aerosol emissions could affect the radiation balance of the Earth–atmosphere system and cause changes in large-scale circulation patterns<sup>18–21</sup>. The abatement of anthropogenic aerosol emissions under China's carbon neutrality will result in additional increases in effective radiative forcing at the top of the atmosphere by 0.17 W m<sup>-2</sup> in 2030 and 0.33 W m<sup>-2</sup> in 2060<sup>20</sup>. In summary, the synergistic reductions in anthropogenic CO<sub>2</sub> and aerosol emissions driven by China's carbon neutrality and clean air policies will have a significant impact on future regional and global climate change, thus further affecting solar PV outputs.

<sup>1</sup>State Key Laboratory of Severe Weather Meteorological Science and Technology & Key Laboratory of Atmospheric Chemistry of CMA, Chinese Academy of Meteorological Sciences, Beijing, China. <sup>2</sup>Climate Change Research Center, Institute of Atmospheric Physics, Chinese Academy of Sciences, Beijing, China.

✉ e-mail: wangzli@cma.gov.cn; leiyd@cma.gov.cn

Many studies have assessed the impact of future climate change on global and regional solar PV potential ( $PV_{POT}$ ) based on simulations conducted under the Representative Concentration Pathways (RCPs)<sup>10,22–25</sup> and Shared Socioeconomic Pathways (SSPs)<sup>26–30</sup> that consider different degrees of socioeconomic development. Although the latest SSPs have provided a relatively comprehensive picture of the future atmospheric composition<sup>1</sup>, they are likely to have overestimated the anthropogenic aerosol emissions in China while not sufficiently considering the characteristics of change in future  $CO_2$  concentrations in China after the first peak and then the attainment of neutrality<sup>31–33</sup>. Moreover, most previous studies have only focused on the changes in average solar PV outputs. For example, Qin et al.<sup>34</sup> and Ren et al.<sup>35</sup> found that the mitigation of aerosols under China’s carbon neutrality would significantly increase  $PV_{POT}$  in China. However, extremely low PV outputs have a large impact on energy security relative to the changes in average PV outputs, and extreme power shortages have increased in recent decades<sup>36</sup>. Therefore, there is an urgent need to assess comprehensively the impact of anthropogenic emission reductions in the context of China’s carbon neutrality on solar  $PV_{POT}$  and projected extremely low PV outputs. This will provide an important scientific basis for the long-term planning and effective utilization of renewable energy both globally and in China.

Here, we conduct two fully coupled transient ensemble simulations using the Community Earth System Model version 2 (CESM2) under the SSP2-4.5 (SSP245) scenario and the combination scenario (CNCN) of the SSP245 and China’s on-time peak-net zero-clean air pathway. A multivariate bias correction algorithm (MBCn) is applied to correct the simulated variables including the downwelling solar flux at the surface (FSDS), surface air temperature (TAS), and surface wind speed (SfcWind). We explore comprehensively the impacts of climate change in the context of China’s carbon neutrality on  $PV_{POT}$  and the projected extremely low PV outputs during the mid-21st century (2041–2060) relative to a reference period (1995–2014) and their potential drivers. Three indices are used to measure the extremely low PV outputs: the proportion of days with extremely low PV outputs ( $PV_{10}$ ), the number of extremely low PV output events ( $PV_{10N}$ ),

and the maximum number of consecutive days with extremely low PV outputs ( $PV_{10D}$ ).

## Results

### Changes in $CO_2$ concentrations and AOD

The simulated global mean  $CO_2$  concentration displays a continuous upward trend in the future under both the SSP245 and CNCN scenarios, reaching ~543.1 and 535.1 ppm by 2060, respectively (Fig. 1a). The global mean  $CO_2$  concentration during the mid-21st century increases by 119.3 and 115.7 ppm under the SSP245 and CNCN scenarios relative to 1995–2014, respectively. Compared to the SSP245 scenario, the global mean  $CO_2$  concentration during the mid-21st century decreased by 3.6 ppm under the CNCN scenario. Unlike the long-lived  $CO_2$ , the AOD averaged over land from 60°S to 60°N displays a fluctuating downward trend under both scenarios due to the reduction of anthropogenic emissions (Fig. 1b). The mean AOD during the mid-21st century decreases -8.3% under the SSP245 scenario and -8.9% under the CNCN scenario relative to 1995–2014. Additionally, the spatial distribution of AOD displays different trends (Fig. 1c, d). The most significant decreases in AOD occur in eastern China, western Europe, and southeastern North America under both scenarios. In contrast, there are different amplitudes of increase in the AOD in Australia, India, and central and southern Africa. The spatial changes of AOD are similar to those under SSP245 using multi-model ensemble simulations<sup>26</sup>. Comparing the CNCN and SSP245 scenarios, the response of AOD to China’s carbon neutrality and clean air policies occurs not only in the local region but also in many other regions, such as Australia, which in turn has an impact on the global and regional climates (Fig. 1e).

### Changes in meteorological factors

Changes in global  $CO_2$  and AOD significantly affect the meteorological factors associated with PV outputs (Fig. 2). Relative to the reference period, the FSDS increases in eastern China, western Europe, eastern North America, and northern South America, while it decreases in northern Africa, western North America, and southern South America under both the SSP245 and CNCN scenarios during the mid-21st century (Fig. 2a, b).

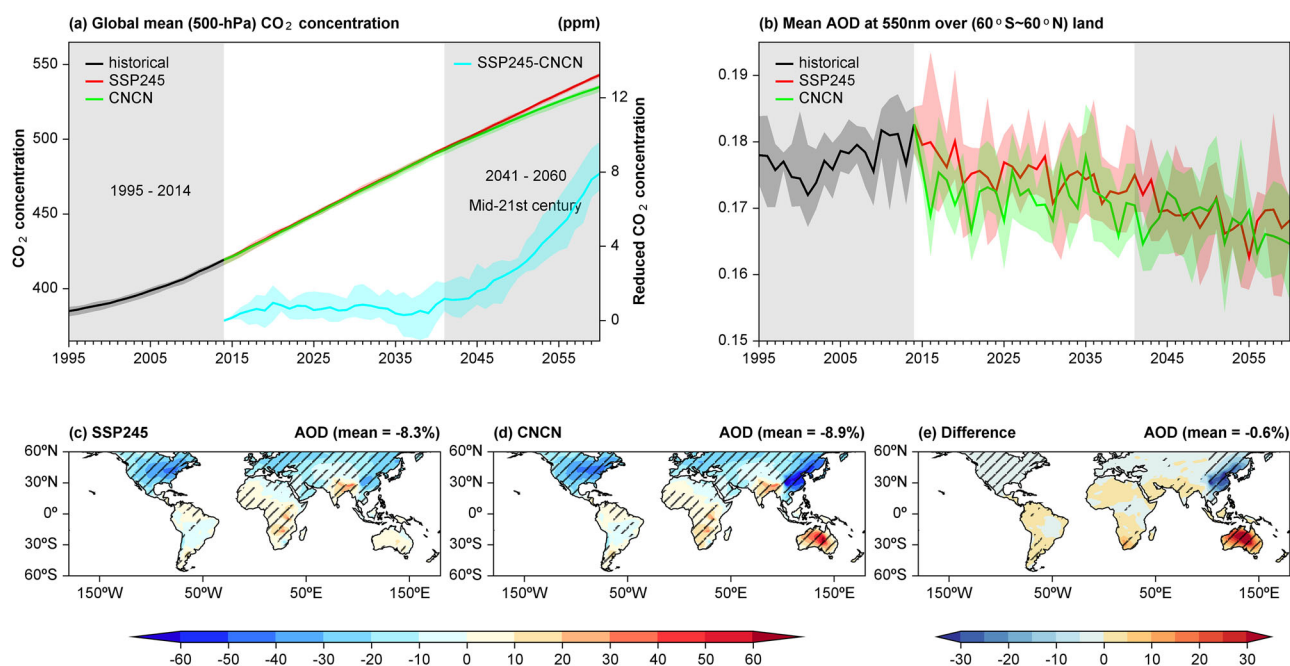


**Fig. 1 | The changes in the  $CO_2$  concentration and AOD.** a Time series of global annual mean (500-hPa)  $CO_2$  concentration (units: ppm) and b 60°S–60°N land mean AOD (unitless) for the historical (1995–2014) and future (2015–2060) scenarios (SSP245 and CNCN). The shaded area covers the range of the five ensemble members’ projected values. Spatial patterns of the relative changes (units: %) in AOD

during the mid-21st century (2041–2060) under the c SSP245 and d CNCN scenarios relative to 1995–2014, and e the difference in the relative changes of AOD between the two scenarios (CNCN and SSP245). Hatched regions indicate that at least four of the five members agree on the sign.

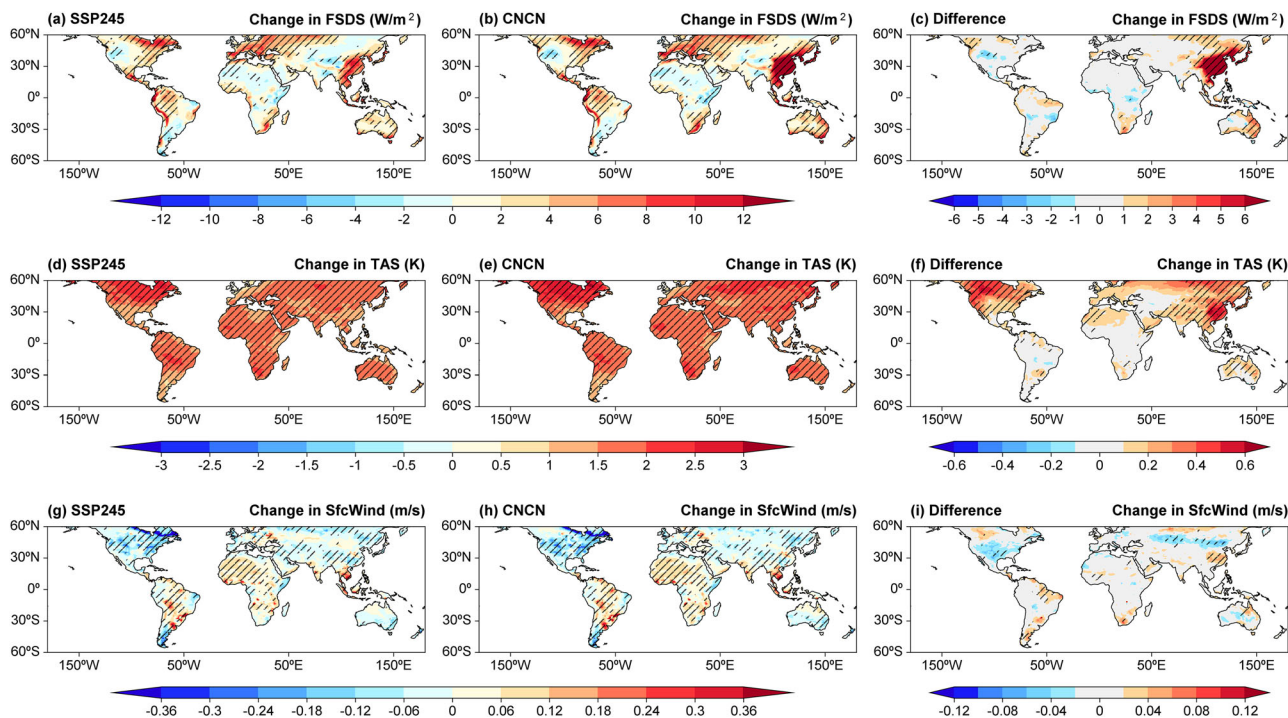


**Fig. 2 | The changes in meteorological factors under different scenarios.** Spatial patterns of changes in (a, b) FSDS (units:  $W\ m^{-2}$ ), (d, e) TAS (units: K), and (g, h) SfcWind (units:  $m\ s^{-1}$ ) during the mid-21<sup>st</sup> century (2041–2060) under the SSP245 and CNCN scenarios relative to 1995–2014. The difference in changes for (c) FSDS, (f) TAS, and (i) SfcWind between the two scenarios (CNCN and SSP245). Hatched regions indicate that at least four of the five members agree on the sign.

Despite their similar spatial distributions, the magnitude of the changes in FSDS differs between the two scenarios. Compared to the SSP245 scenario, the abatement in anthropogenic emissions driven by China’s carbon neutrality and clean air policies results in significant increases in FSDS over some regions in the mid-low latitude continents (Fig. 2c). The largest regional increase in FSDS is observed in East Asia, with a value of  $5.9\ W\ m^{-2}$ . The changes in FSDS are not completely inversely correlated with those in AOD, which is mainly attributed to the influence of cloud cover and other atmospheric components (e.g., water vapor) on FSDS<sup>30</sup>.

The increases in TAS exceed 1.5 K across most of the mid-low latitude continents, with a large inter-member consistency under both the SSP245 and CNCN scenarios (Fig. 2d, e). The differences in the changes of TAS between the two scenarios indicate that the abatement of anthropogenic CO<sub>2</sub> and aerosol emissions in the context of China’s carbon neutrality not only causes local warming but also induces additional warming in some remote regions during the mid-21<sup>st</sup> century (Fig. 2f). The local warming is mainly attributed to aerosol emission reductions driven by China’s carbon neutrality and clean air policies. The CO<sub>2</sub> emission reductions can decrease TAS, but aerosol emission reductions cause strong local warming, offsetting the cooling effects of CO<sub>2</sub> mitigation. Moreover, the additional warming in remote regions, including North America, Europe, and Australia, can be attributed to multiple factors (Supplementary Fig. 1). Specifically, the warming in North America and Europe is mainly due to the increase in the net radiation flux at the surface caused by the decrease in total cloud cover and the increase in surface humidity. The increased surface humidity in North America and Europe during the mid-21<sup>st</sup> century under the CNCN scenario may be attributed to the increased wind speed over the North Pacific and North Atlantic, transporting more water vapor to North America and Europe. For India and Australia, the increase of TAS is mainly associated with the decrease in total cloud cover leading to the increase in the net radiation flux at the surface. Noteworthy, the warming in remote regions driven by aerosol emission reductions in China is also reported by an early study<sup>20</sup>. Additionally, the SfcWind decreases in southern Australia, most of Eurasia, North America, and southern South America, but increases in parts of Africa, South America, and southeastern Asia under both the SSP245 and

CNCN scenarios during the mid-21<sup>st</sup> century relative to the reference period (Fig. 2g, h). The difference in the changes for SfcWind between the two scenarios shows that the abatement in anthropogenic emissions in the context of China’s carbon neutrality mainly increases SfcWind in eastern China, southern Africa, and eastern and southern South America, while it decreases SfcWind in central Eurasia and southern North America (Fig. 2i).

### Changes in PV<sub>POT</sub>

Changes in meteorological factors also have an impact on the PV<sub>POT</sub> (Fig. 3). At the regional scale, the mean PV<sub>POT</sub> significantly increases in eastern China, western Europe, eastern North America, and northern South America, whereas it significantly decreases in India, northern Africa, western North America, and southern South America under both scenarios (Fig. 3a, b). The signs of the regional PV<sub>POT</sub> changes align with the results obtained under SSP245 based on multiple models<sup>26,37</sup>.

Comparing the changes in PV<sub>POT</sub> during the mid-21<sup>st</sup> century between the two scenarios, we find that the inter-scenario differences in PV<sub>POT</sub> changes have a similar spatial distribution to those of the FSDS changes (Figs. 2c and 3c). Relative to the SSP245 scenario, changes in FSDS, TAS, and SfcWind caused by the anthropogenic emission reductions in the context of China’s carbon neutrality significantly strengthen the PV<sub>POT</sub> over some regions in the mid-low latitude continents (Fig. 3c, d). The region with the largest enhancement in PV<sub>POT</sub> is located in East Asia, with an additional increase of ~3.3% (from 1.5% under the SSP245 scenario to 4.8% under the CNCN scenario). Among them, the most significant enhancement in PV<sub>POT</sub> in eastern China suggests that there is positive feedback between the anthropogenic emission reductions and the increases in PV<sub>POT</sub> in China, which is conducive to accelerating the realization of China’s carbon neutrality target. Previous studies<sup>34,37</sup> have reported similar results. The next largest enhancements in PV<sub>POT</sub> occur in eastern Australia and northern Asia, reaching about 0.9% and 0.8%, respectively. Moreover, the enhancement in PV<sub>POT</sub> also can be found in South Asia (0.2%), southern Africa (0.3%), western Europe (0.2%), and eastern South America (0.5%), where large-scale PV plants are built. Therefore, China’s carbon neutrality and

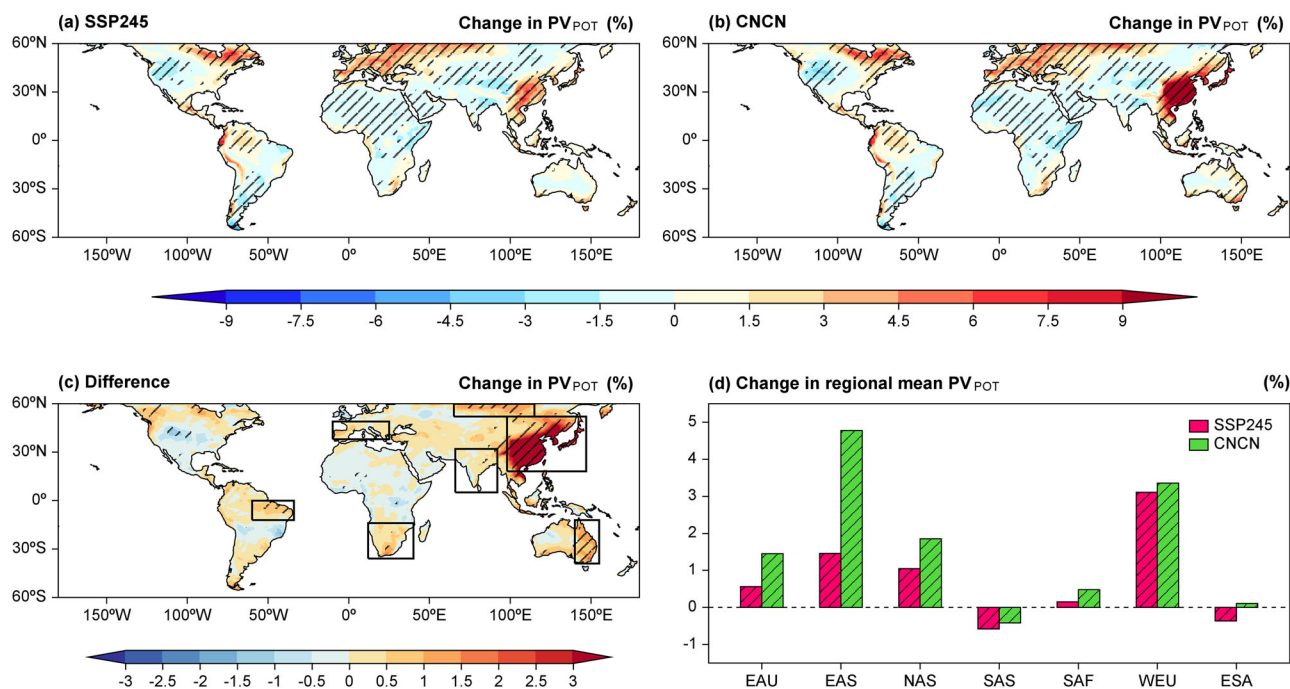


**Fig. 3 | The changes in PV<sub>POT</sub> under different scenarios.** Spatial patterns of the relative changes in PV<sub>POT</sub> (units: %) during the mid-21<sup>st</sup> century (2041–2060) under a SSP245 and b CNCN scenarios relative to 1995–2014, and c the difference in the relative changes of PV<sub>POT</sub> between the two scenarios (CNCN and SSP245). Hatched regions indicate that at least four of the five members agree on the sign. d Relative

changes in the PV<sub>POT</sub> in eastern Australia (EAU), East Asia (EAS), northern Asia (NAS), South Asia (SAS), southern Africa (SAF), western Europe (WEU), and eastern South America (ESA) during the mid-21<sup>st</sup> century under the SSP245 and CNCN scenarios relative to 1995–2014. Hatched bars indicate that at least four of the five members agree on the sign.

clean air policies not only enhance local PV<sub>POT</sub> but also have a positive effect on PV<sub>POT</sub> in some other regions of the world.

We analyze further the relative contributions of various meteorological factors to the changes in PV<sub>POT</sub> (Fig. 4). There is a larger contribution from FSDS and TAS than from SfcWind to the changes in PV<sub>POT</sub> under the SSP245 (Fig. 4a, d, g) and CNCN (Fig. 4b, e, h) scenarios during the mid-21<sup>st</sup> century relative to the reference period. This result is consistent with those of previous studies<sup>22,37</sup>. The increase in FSDS dominates the increase in PV<sub>POT</sub> in regions with significantly increased PV<sub>POT</sub> during the mid-21<sup>st</sup> century relative to the reference period, including eastern China, western Europe, eastern North America, and northern South America, and the increase in TAS has a relatively minor impact on PV<sub>POT</sub> changes. However, the decrease in FSDS and increase in TAS dominate the decrease in PV<sub>POT</sub> in regions with significantly decreased PV<sub>POT</sub> during the mid-21<sup>st</sup> century relative to the reference period, including India, northern Africa, and western North America. When comparing the variations in PV<sub>POT</sub> between the two scenarios, it is notable that FSDS plays a significantly more substantial role than TAS and SfcWind (Fig. 4c, f, i). The FSDS changes from anthropogenic emission reductions driven by China’s carbon neutrality and clean air policies dominate the difference in PV<sub>POT</sub> changes between the two scenarios over almost the entire mid-low latitude continental area, with strong agreement among ensemble members. This explains why there are very similar spatial patterns in the differences between the changes in PV<sub>POT</sub> and FSDS under the two scenarios. Therefore, the abatement in anthropogenic CO<sub>2</sub> and aerosol emissions in the context of China’s carbon neutrality affects the PV<sub>POT</sub> mainly by changing the FSDS.

### Changes in extremely low PV outputs

Extreme PV outputs can have a substantial impact on energy security. The changes in extremely low PV outputs during the mid-21<sup>st</sup> century relative to the reference period are further analyzed based on three PV output indices: PV10, PV10N, and PV10D (Fig. 5). Under the SSP245 (Fig. 5a, d, g) and CNCN (Fig. 5b, e, h) scenarios, PV10, PV10N, and PV10D decrease in regions with significantly increased PV<sub>POT</sub>, including eastern China,

western Europe, eastern North America, and northern South America. This suggests that future solar PV outputs in these regions will become stronger and more stable. However, PV10, PV10N, and PV10D increase in regions with significantly decreased PV<sub>POT</sub>, including India, northern Africa, and western North America, suggesting that future solar PV outputs in these regions will decrease and become less stable. The increases in PV10, PV10N, and PV10D are more significant in northern Africa.

The abatement in anthropogenic emissions in the context of China’s carbon neutrality reduces the PV10, PV10N, and PV10D over some regions in the mid-low latitude continents, suggesting that China’s carbon neutrality and clean air policies have a positive effect on improving the stability of PV outputs in these regions (Fig. 5c, f, i). The largest decreases in PV10, PV10N, and PV10D occur in East Asia, reaching −24.8%, −33.5%, and −14.9%, respectively. In particular, there are most pronounced improvements in the extremely low PV outputs in eastern China. More stable PV power generation in eastern China in the future would be conducive to meeting the increased demand for electricity and energy transition. This will further promote the positive feedback between emission reductions and solar PV power generation. Additionally, China’s carbon neutrality and clean air policies also lead to obvious improvements in the extremely low PV outputs in eastern Australia, South Asia, southern Africa, and eastern South America, with PV10 decreasing by about −7.2%, −5.5%, −5.5%, and −8.3%, PV10N decreasing by about −11.9%, −9.7%, −12.5%, and −20.2%, and PV10D decreasing by about −4.1%, −5.3%, −4.7%, and −8.8%, respectively.

We separate the contributions of three meteorological factors, FSDS, TAS, and SfcWind, to the extremely low PV outputs (Fig. 6 and Supplementary Figs. 2 and 3). The FSDS and TAS contribute more than SfcWind to the changes in PV10 under the SSP245 (Fig. 6a, d, g) and CNCN (Fig. 6b, e, h) scenarios during the mid-21<sup>st</sup> century relative to the reference period. The increase in FSDS dominates the decrease in PV10, in regions with significantly decreased PV10, including eastern China, western Europe, eastern North America, and northern South America, while the decrease in FSDS and the increase in TAS dominate the increase in PV10 in regions with

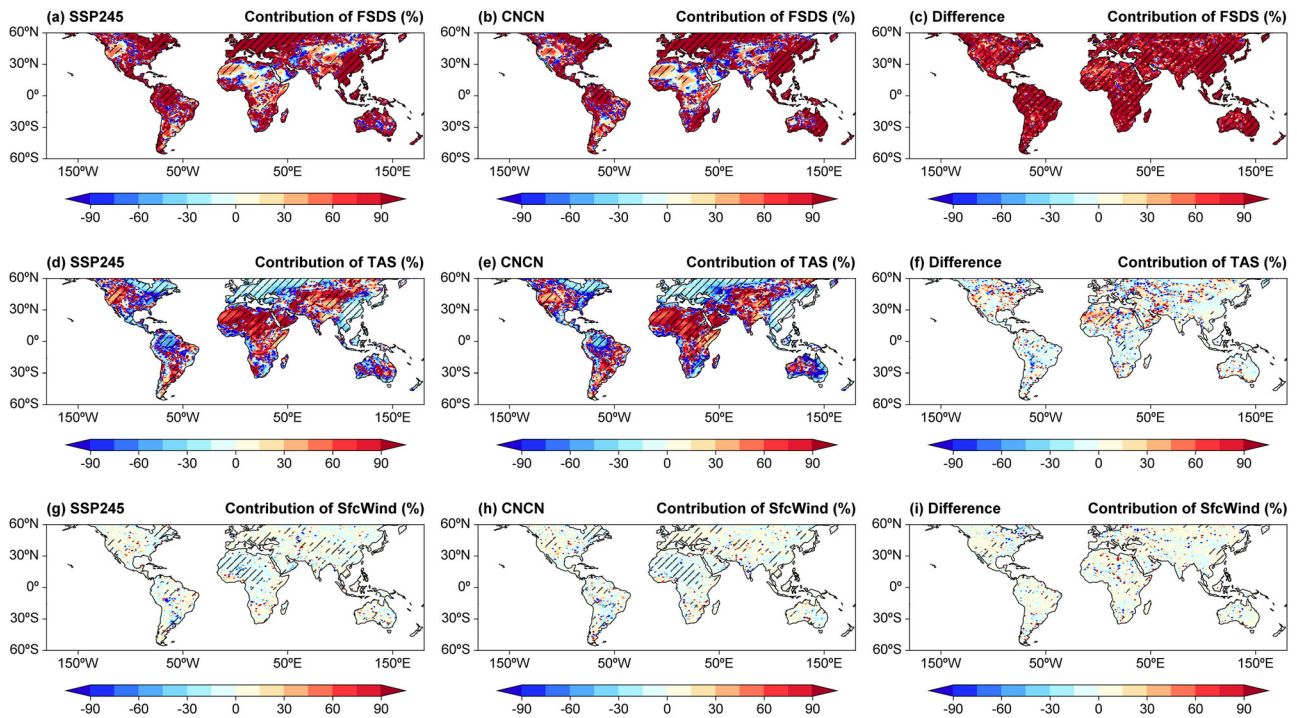


**Fig. 4 | The relative contribution of meteorological factors to changes in  $PV_{POT}$ .** The relative contribution (units: %) of **a, b** FSDS, **d, e** TAS, and **g, h** SfcWind to changes in  $PV_{POT}$  during the mid-21<sup>st</sup> century (2041–2060) under the SSP245 and CNCN scenarios relative to 1995–2014. The relative contribution of **c** FSDS, **f** TAS, and **i** SfcWind to the difference in changes for  $PV_{POT}$  between the two scenarios (CNCN and SSP245). Hatched regions indicate that at least four of the five members agree on the sign.

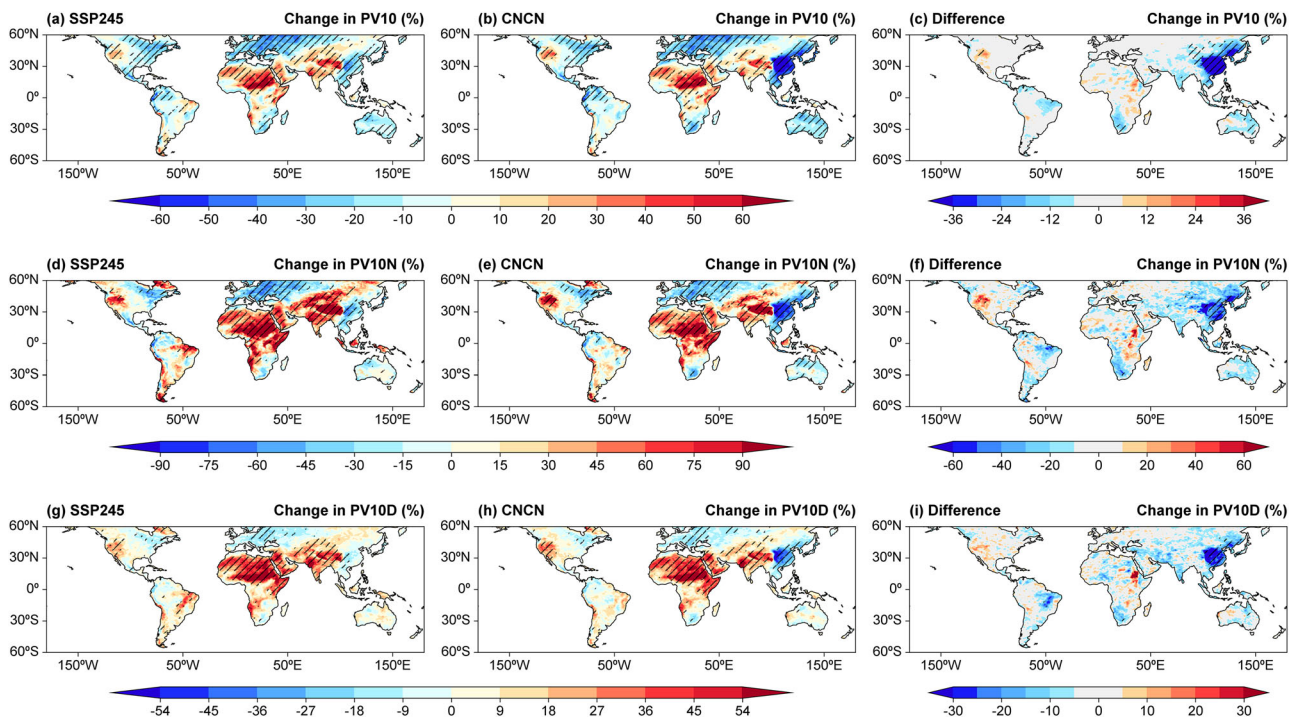


**Fig. 5 | The changes in extremely low PV outputs under different scenarios.** Spatial patterns of the relative changes (units: %) in **a, b** PV10, **d, e** PV10N, and **g, h** PV10D during the mid-21<sup>st</sup> century (2041–2060) under the SSP245 and CNCN scenarios relative to 1995–2014. The difference in the relative changes of **c** PV10, **f** PV10N, and **i** PV10D between the two scenarios (CNCN and SSP245). Hatched regions indicate that at least four of the five members agree on the sign.

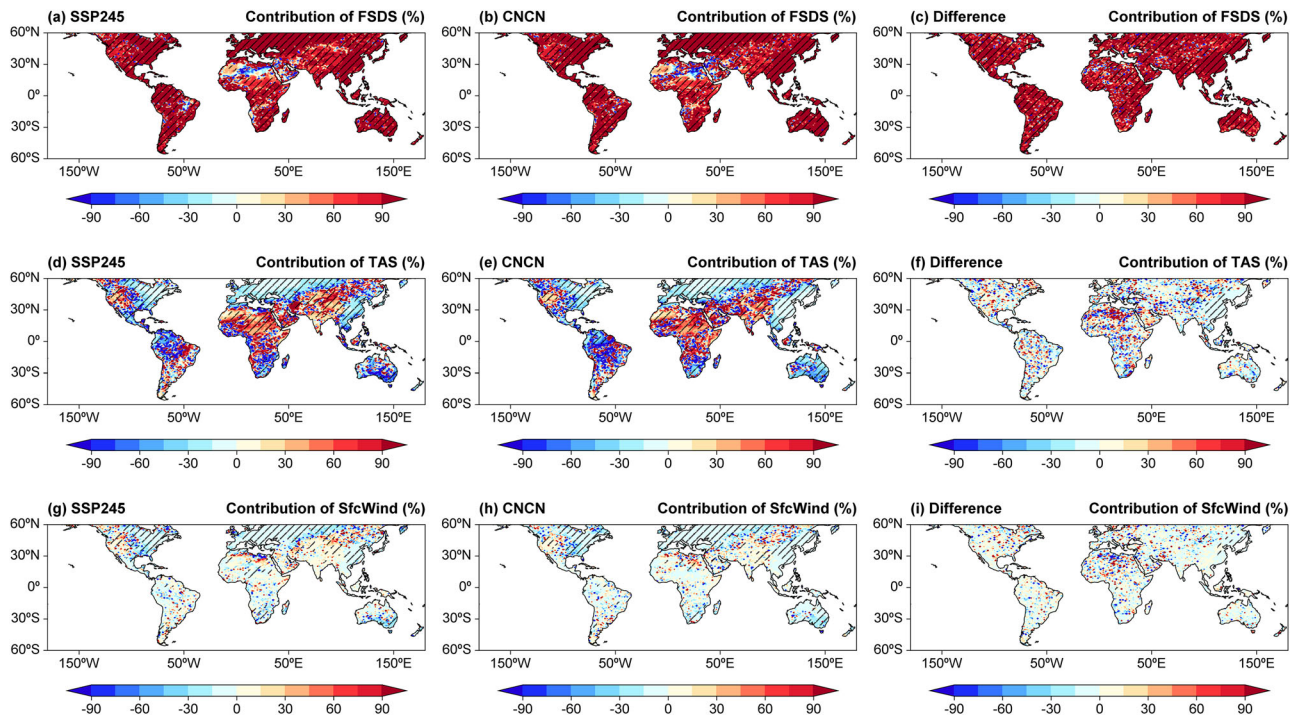


**Fig. 6 | The relative contribution of meteorological factors to the changes in PV10.** The relative contribution (units: %) of **a, b** FSDS, **d, e** TAS, and **g, h** SfcWind to changes in PV10 during the mid-21<sup>st</sup> century (2041–2060) under the SSP245 and CNCN scenarios relative to 1995–2014. The relative contribution of

**c** FSDS, **f** TAS, and **i** SfcWind to the difference in changes for PV10 between the two scenarios (CNCN and SSP245). Hatched regions indicate that at least four of the five members agree on the sign.

significantly increased PV10, including India, northern Africa, and western North America. Comparing the differences in PV10 changes between the two scenarios, the contribution of FSDS is significantly greater than that of TAS and SfcWind (Fig. 6c, f, i). The changes in FSDS driven by China’s carbon neutrality and clean air policies dominate the changes in PV10 in almost the entire mid-low latitude continental area. The relative contributions of TAS and SfcWind are much less than that of FSDS, and the agreement among ensemble members is poor in most regions. Similar results are obtained for PV10N and PV10D (Supplementary Figs. 2 and 3). Thus, as for PV<sub>POT</sub>, changes in anthropogenic CO<sub>2</sub> and aerosol emissions in the context of China’s carbon neutrality improve the extremely low PV outputs mainly by changing the FSDS.

### Discussion

Our results indicate that the abatement in anthropogenic emissions in the context of China’s carbon neutrality will enhance PV<sub>POT</sub> and decrease the extremely low PV outputs in the future over some regions in the mid-low latitude continents. In East Asia, the enhanced PV<sub>POT</sub> and reduced extremely low PV outputs are the most significant. In particular, the greatest enhancement of PV<sub>POT</sub> and the largest decrease in extremely low PV outputs are both found in eastern China, indicating strong positive feedback between local emission reductions and the enhancement of PV<sub>POT</sub> and its stability. The enhanced PV power in eastern China from emission reductions driven by China’s carbon neutrality and clean air policies will increase the local power supply capacity and reduce the dependence on west-to-east power transmission to support the high energy demand in the most populated region of China. Moreover, this study also identifies the positive effects of the abatements in anthropogenic emissions driven by China’s carbon neutrality and clean air policies on PV power generation in some other regions of the world, including eastern Australia, South Asia, southern Africa, and eastern South America. Considering that these regions are experiencing rapid solar PV installation rates or have large total cumulative installed capacities, the emission reductions in the context of China’s carbon neutrality will be extremely beneficial for enhancing its PV power efficiency.

Compared with an early study by Ren et al.<sup>35</sup>, which concerns the renewable benefits from aerosol mitigation in China, our study provides some new insights: (1) Our study provides a comprehensive assessment of PV benefits from anthropogenic emission changes in the context of China’s carbon neutrality, including CO<sub>2</sub> and aerosol, rather than only aerosol mitigation in ref. 35; (2) Compared to previous most studies<sup>24,34,35,37</sup>, focusing on only mean state of PV outputs, our study also analyzes the changes of extremely low PV outputs using appropriate indices and reveals the co-benefits of China’s carbon neutrality and clean air policies in increasing the PV<sub>POT</sub> and reducing the occurrence of extremely low PV outputs; (3) Compared to a regional assessment by Ren et al.<sup>35</sup>, our global assessment demonstrates that China’s carbon neutrality and clean air policies will not only trigger local positive feedback between anthropogenic emission reductions and PV increases but will also generate additional PV enhancements in some remote regions.

There are some limitations and uncertainties in this study. (1) Although this study applies MBCn to reduce the uncertainty in model simulations, only one Earth system model is adopted in the simulation experiments, which will still leave some uncertainty in the projections. (2) We use a simplified parameterization to calculate PV<sub>POT</sub>. This scheme only considered the effects of FSDS, TAS, and SfcWind on PV outputs, while neglecting some possible influences, such as solar altitude and PV tilt angles<sup>38</sup>. (3) Although it is found that the increase in FSDS is the predominant factor that enhanced PV power in the context of China’s carbon neutrality, the individual contributions of changes in AOD and cloud cover to the increased FSDS remain unclear. Based on surface solar radiation under full sky and clear sky conditions, Wang et al.<sup>39</sup> found that the trend of FSDS changes was dominated by AOD changes, and the influence of cloud cover changes was relatively limited. A correlation analysis conducted by Zou et al.<sup>10</sup> revealed that the decreased AOD was the main cause of future PV increases in East Asia under RCP8.5. The physical mechanism by which anthropogenic emission reductions affect PV outputs in the context of China’s carbon neutrality requires further investigation.

**Table 1 | Experimental design**

Experiment name	Simulation period	Ensemble member	Scenario description
EXP_SSP245	2015–2060	5	Global anthropogenic emissions for CO <sub>2</sub> , SO <sub>2</sub> , sulfate, BC, POM, and SOAG are from SSP2-4.5.
EXP_CNCN			Anthropogenic emission data for CO <sub>2</sub> , SO <sub>2</sub> , sulfate, BC, POM, and SOAG in the Chinese mainland are from MEICv1.4 and DPECv1.2; the corresponding anthropogenic emissions in other regions are from SSP2-4.5.

Despite these limitations and uncertainties, our results remain quite valuable for informing the strategic planning and implementation of solar PV systems in the context of achieving carbon neutrality. By quantifying the impact of abatement in anthropogenic emissions in the context of China's carbon neutrality on global PV outputs, this study confirms that emission reductions will not only result in positive feedback effects between local anthropogenic emission reductions and PV enhancements but will also enhance PV power generation in some other regions of the world.

## Methods

### Data

Anthropogenic emissions of CO<sub>2</sub> and major air pollutants, including sulfur dioxide (SO<sub>2</sub>), sulfate, black carbon (BC), primary organic matter (POM), and secondary organic aerosol gaseous (SOAG) precursors in the Chinese mainland under the carbon neutrality target used in this study, are obtained from the on-time peak-net zero-clean air pathway simulated by the Dynamic Prediction model for Emissions in China (DPECv1.2) developed by Tsinghua University. Under this pathway, China will achieve peak carbon by 2030, achieve carbon neutrality by 2060, and continuously adopt the most optimal end-of-pipe pollution control measures<sup>17</sup>. Because the range of emission data provided by DPECv1.2 is 2020–2060, this study uses the anthropogenic emission data provided by the Multi-resolution Emission Inventory for China (MEICv1.4) to supplement the emission data for CO<sub>2</sub> and major air pollutants in the Chinese mainland from 2015 to 2019. Other than the anthropogenic source emissions, all other data for 2015–2060 used in the simulation experiments, such as natural source emissions, are taken from the SSP2-4.5 scenario. The daily FSDS, TAS, and SfcWind for 1995–2014 are modeled using CESM2 default historical data. Additionally, the hourly FSDS, TAS, and SfcWind for 1995–2014 from the European Centre for Medium-Range Weather Forecasts Reanalysis 5 (ERA5) are used to correct the simulated results. This dataset has a spatial resolution of 0.25° × 0.25°, and we interpolate it to grids with a spatial resolution of 0.9° × 1.25°, to allow for the bias correction of model outputs.

### The Earth system model and experimental design

Earth system models are important tools for projecting future climate change<sup>40</sup>. In this study, CESM2 is used to conduct sensitivity experiments. Compared to CESM1, the simulations of temperature, radiation, and many other metrics have been significantly improved in CESM2. Among the coupled models in CMIP6, it is one of the most closely aligned to observational data. The CESM2 consists of an atmosphere model (CAM6/WACCM6), ocean model (POP2), land model (CLM5), sea-ice model (CICE5), land-ice model (CISM2), wave model (WW3), river model (MOSART), and a coupler (CIME5)<sup>41</sup>. In this study, the fully-coupled model CESM2 is used to conduct sensitivity simulation experiments. Its atmospheric component (CAM6) is compiled with a horizontal resolution of a nominal 1° (0.9° in latitude and 1.25° in longitude), 32 vertical levels, and a model top ~40 km above the surface<sup>41</sup>.

The SSP2-4.5 scenario is a combination of SSP2 (the 21st-century “middle of the road” scenario) and RCP4.5 (a medium forcing with a total anthropogenic radiative forcing of 4.5 W m<sup>-2</sup> in 2100), in which GHG emissions remain around current levels until they begin to decline in the middle of the century but do not reach net zero in 2100, and the global mean temperature rise is ~2.6 °C by the end of the century<sup>42,43</sup>. Compared to the other SSPs, SSP2-4.5 depicts historical CO<sub>2</sub> emission trends that are closest to recent reality and depicts future CO<sub>2</sub> and air pollutant emissions and land

use levels that are not extreme<sup>42–44</sup>. Thus, SSP2-4.5 is defined as the reference scenario (SSP245). Moreover, we define a new CNCN scenario by replacing the anthropogenic emissions of the SSP245 scenario in the Chinese mainland with anthropogenic emissions from DPECv1.2, which takes into account the abatement in anthropogenic CO<sub>2</sub> and aerosol emissions in the context of China's carbon neutrality. In particular, the reduction of anthropogenic aerosol emissions is driven by both carbon neutrality and clean air policies in China. The simulation experiments conducted under the two scenarios use restart files from historical simulations for the period 1990–2014 and are denoted as EXP\_SSP245 and EXP\_CNCN, respectively. The difference between the two sets of experiments is that anthropogenic CO<sub>2</sub> and major aerosol emissions in the Chinese mainland during 2015–2060 are derived from SSP2-4.5 in EXP\_SSP245, while they are derived from MEICv1.4 and DPECv1.2 in EXP\_CNCN. Compared to the SSP245 scenario, the SO<sub>2</sub>, sulfate, BC, and POM emissions show greater declines in China during the mid-21<sup>st</sup> century under the CNCN scenario relative to 1995–2014 (Supplementary Figs. 4–7). Especially for BC and POM, the decline is more than 90% in China during the mid-21<sup>st</sup> century under the CNCN scenario, while it is no more than 45% under the SSP245 scenario. Moreover, anthropogenic SOAG and CO<sub>2</sub> emissions in China during the mid-21<sup>st</sup> century decreased under the CNCN scenario, while increasing under the SSP245 scenario, relative to 1995–2014 (Supplementary Figs. 8 and 9). These emission differences between the SSP245 and CNCN scenarios are driven by China's carbon neutrality and clean air policies, which will ultimately affect PV power generation by changing meteorological factors. All emissions, except for the anthropogenic emissions referred to above, such as those from biomass burning, and volcanic eruptions, and the other model configurations are the same in both sets of experiments. Each set of experiments is conducted with five ensemble members to minimize the effect of model internal variability on the simulation results. The experiments conducted in this study are all transient simulations. The details of the experimental design are shown in Table 1.

### Multivariate bias correction algorithm

To reduce the uncertainty in the simulation results of the Earth System Model, the MBCn<sup>45</sup> is applied to correct the bias of the climate variables in the historical and future simulations. The MBCn is a multivariate form of quantile mapping bias correction, which not only has the advantages of quantile mapping bias correction<sup>46</sup> but also includes the dependencies among different variables. The MBCn can transfer the observed continuous multivariate distribution to the corresponding multivariate distribution of climate variables simulated by the model<sup>45</sup>. When using the MBCn to correct climate model projections, three datasets are required: historical observations, historical simulations, and future projections. ERA5 has been widely used to assess and correct the outputs of Earth system models<sup>28,37,47,48</sup>, therefore, this study uses daily climate variables data from ERA5 during 1995–2014 as its historical observations. The bias correction for historical and future simulations is conducted independently by applying the MBCn R package (<https://rdrr.io/cran/MBCn/man/MBCn.html>) for each ensemble member's outputs. Before the bias correction, the difference in the FSDS between the simulation and observation exceeds 40 W m<sup>-2</sup> in some regions, and both the simulated TAS and SfcWind are overestimated in most regions (Supplementary Figs. 10b, 11b, and 12b). After the bias correction, the simulated deviations of FSDS, TAS, SfcWind, and PV<sub>POT</sub> are significantly decreased on global and regional scales (Supplementary Figs. 10–13).

**Table 2 | Extremely low PV output indices**

Indices name	Indices definition	Units
PV10	The share of days with PV <sub>POT</sub> below the extremely low PV output thresholds.	%
PV10N	The annual number of extremely low PV output events (The extremely low PV output event is defined as PV <sub>POT</sub> below the extremely low PV output thresholds for at least 3 consecutive days).	times
PV10D	The maximum length of consecutive days with PV <sub>POT</sub> below the extremely low PV output thresholds.	days

**The PV<sub>POT</sub> and extremely low PV outputs**

An internationally widely used solar PV<sub>POT</sub> parameterization scheme is used to calculate the PV<sub>POT</sub>. The PV<sub>POT</sub> is defined as the ratio of the solar PV output generated under actual weather conditions to that under standard conditions and is a dimensionless quantity. According to previous studies<sup>22–25,34,35,37,49,50</sup>, the PV<sub>POT</sub> is calculated as follows:

$$PV_{POT} = P_R \frac{I}{I_{STC}} \tag{1}$$

where *I* is FSDS; *I<sub>STC</sub>* is the downwelling solar flux on the PV panel under standard test conditions (1000 W m<sup>-2</sup>); and *P<sub>R</sub>* is the performance ratio, which indicates the influence of cell temperature on the power generation efficiency of the PV panel, and can be calculated as follows:

$$P_R = 1 - \gamma(T_{cell} - T_{STC}) \tag{2}$$

where *γ* represents the impact of the monocrystalline silicon cell on the photoelectric conversion performance ratio and is defined as a constant of 0.005 °C<sup>-1</sup>; *T<sub>cell</sub>* is the cell temperature under actual weather conditions and *T<sub>STC</sub>* is the cell temperature under standard test conditions (25 °C). *T<sub>cell</sub>* above 25 °C reduces the performance ratio, while it below 25 °C improves the performance ratio. *T<sub>cell</sub>* is influenced by FSDS, TAS (*T*), and SfcWind (*V*):

$$T_{cell} = c_1 + c_2 T + c_3 I - c_4 V \tag{3}$$

where *c<sub>1</sub>*, *c<sub>2</sub>*, *c<sub>3</sub>*, and *c<sub>4</sub>* are parameters with values of 4.3 °C, 0.943, 0.028 °C W<sup>-1</sup> m<sup>2</sup>, and 1.528 °C m<sup>-1</sup> s, respectively.

Additionally, the changes in extremely low PV outputs are assessed using the extremely low PV threshold and three related indices (PV10, PV10N, and PV10D; Table 2). To obtain the extremely low PV output threshold, the extreme event occurrence probability assessment approach is adopted<sup>51</sup>. First, we sample the daily PV<sub>POT</sub> for the period 1995–2014 using a 15-day sliding window. After sampling, a set of 300 values could be obtained for any calendar day of the year (15 daily PV<sub>POT</sub> values for each of 7 days before to 7 days after the target day, and 20 samples from 1995–2014 for that calendar day). Then, the probability density function of PV<sub>POT</sub> for the calendar day is obtained from the sampling results for that day, and the value corresponding to the 10th percentile of the distribution is used as the extremely low PV output threshold for that calendar day. Finally, a set of extremely low PV output thresholds is obtained containing 365 values that covered the range of extremely low PV outputs for 1995–2014.

**The relative contribution of the drivers of PV changes**

Changes in PV<sub>POT</sub> and extremely low PV outputs are caused by changes in FSDS, TAS, and SfcWind. To determine the relative contributions of these three drivers to the overall changes in PV<sub>POT</sub> and extremely low PV outputs, the single change factor approach adopted by Feron et al. is utilized<sup>25</sup>. For example, the relative contribution (*RC<sub>proj-hist</sub>*) of FSDS to the change in PV<sub>POT</sub> (or extremely low PV outputs) during the mid-21<sup>st</sup> century relative to

1995–2014 is calculated as follows:

$$RC_{proj-hist} = \frac{PV(I_{proj}, T_{hist}, V_{hist}) - PV(I_{hist}, T_{hist}, V_{hist})}{PV(I_{proj}, T_{proj}, V_{proj}) - PV(I_{hist}, T_{hist}, V_{hist})} \times 100\% \tag{4}$$

where *PV(I<sub>proj</sub>, T<sub>hist</sub>, V<sub>hist</sub>)* are the PV<sub>POT</sub> (or three extremely low PV output indices) calculated from FSDS (*I<sub>proj</sub>*) for the mid-21<sup>st</sup> century and TAS (*T<sub>hist</sub>*) and SfcWind (*V<sub>hist</sub>*) for 1995–2014; *PV(I<sub>hist</sub>, T<sub>hist</sub>, V<sub>hist</sub>)* are the PV<sub>POT</sub> (or three extremely low PV output indices) calculated from FSDS (*I<sub>hist</sub>*), TAS (*T<sub>hist</sub>*), and SfcWind (*V<sub>hist</sub>*) for 1995–2014; and *PV(I<sub>proj</sub>, T<sub>proj</sub>, V<sub>proj</sub>)* are the PV<sub>POT</sub> (or three extremely low PV output indices) calculated from FSDS (*I<sub>proj</sub>*), TAS (*T<sub>proj</sub>*), and SfcWind (*V<sub>proj</sub>*) for the mid-21<sup>st</sup> century.

Additionally, we calculate the relative contribution (*RC<sub>CNCN-SSP245</sub>*) of FSDS to the difference in the change for PV<sub>POT</sub> (or extremely low PV outputs) between the two scenarios as follows:

$$RC_{CNCN-SSP245} = \frac{PV(I_{CNCN}, T_{SSP245}, V_{SSP245}) - PV(I_{SSP245}, T_{SSP245}, V_{SSP245})}{PV(I_{CNCN}, T_{CNCN}, V_{CNCN}) - PV(I_{SSP245}, T_{SSP245}, V_{SSP245})} \times 100\% \tag{5}$$

where *PV(I<sub>CNCN</sub>, T<sub>SSP245</sub>, V<sub>SSP245</sub>)* are the PV<sub>POT</sub> (or three extremely low PV output indices) calculated from FSDS (*I<sub>CNCN</sub>*) for the mid-21<sup>st</sup> century under the CNCN scenario and TAS (*T<sub>SSP245</sub>*) and SfcWind (*V<sub>SSP245</sub>*) for the mid-21<sup>st</sup> century under the SSP245 scenario; *PV(I<sub>SSP245</sub>, T<sub>SSP245</sub>, V<sub>SSP245</sub>)* are the PV<sub>POT</sub> (or three extremely low PV output indices) calculated from FSDS (*I<sub>SSP245</sub>*), TAS (*T<sub>SSP245</sub>*), and SfcWind (*V<sub>SSP245</sub>*) for the mid-21<sup>st</sup> century under the SSP245 scenario; and *PV(I<sub>CNCN</sub>, T<sub>CNCN</sub>, V<sub>CNCN</sub>)* are the PV<sub>POT</sub> (or three extremely low PV output indices) calculated from FSDS (*I<sub>CNCN</sub>*), TAS (*T<sub>CNCN</sub>*), and SfcWind (*V<sub>CNCN</sub>*) for the mid-21<sup>st</sup> century under the CNCN scenario. The relative contributions of TAS and SfcWind to the changes in PV<sub>POT</sub> (or extremely low PV outputs) are obtained using the same method.

**Definition of sub-regions**

Seven sub-regions of interest are selected for investigation: eastern Australia (EAU; 140°E–155°E, 39°S–12°S), East Asia (EAS; 98°E–147°E, 18°N–52°N), northern Asia (NAS; 65°E–115°E, 52°N–60°N), South Asia (SAS; 66°E–92°E, 5°N–32°N), southern Africa (SAF; 12°E–40°E, 36°S–14°S), western Europe (WEU; 10°W–25°E, 38°N–49°N), and eastern South America (ESA; 60°W–34°W, 12°S–0°). Almost every sub-region has a rapid solar PV installation rate or large PV installed capacities. These sub-regions are marked with black boxes in Fig. 3a.

**Data Availability**

The emission inventories from MEICv1.4 and DPECv1.2 are freely available at <http://meicmodel.org.cn>. The meteorological datasets for 1995–2014 from ERA5 are freely available at <https://www.ecmwf.int/en/forecasts/dataset/ecmwf-reanalysis-v5>. The simulation data from CESM2 are available upon request from the corresponding author.

Received: 5 September 2024; Accepted: 13 March 2025;  
Published online: 27 March 2025

## References

- IPCC. Summary for Policymakers. In: Climate Change 2023: Synthesis Report. Contribution of Working Groups I, II, and III to the Sixth Assessment Report of the Intergovernmental Panel on Climate Change [Core Writing Team, Lee, H., and Romero, J. (eds.)]. (IPCC, 2023).
- Zhao, C., Brissette, F. & Chen, J. Projection of future extreme meteorological droughts using two large multi-member climate model ensembles. *J. Hydrol.* **618**, 129155 (2023).
- Ridder, N. N., Ukkola, A. M., Pitman, A. J. & Perkins-Kirkpatrick, S. E. Increased occurrence of high impact compound events under climate change. *npj Clim. Atmos. Sci.* **5**, 3 (2022).
- UNFCCC. Report of the Conference of the Parties on its twenty-first session, held in Paris from 30 November to 11 December 2015. Addendum. Part two: Action taken by the Conference of the Parties at its twenty-first session (2015).
- Zhang, Q. et al. Synergetic roadmap of carbon neutrality and clean air for China. *Environ. Sci. Ecotechnol.* **16**, 100280 (2023).
- Huang, M.-T. & Zhai, P.-M. Achieving Paris Agreement temperature goals requires carbon neutrality by middle century with far-reaching transitions in the whole society. *Adv. Clim. Chang. Res.* **12**, 281–286 (2021).
- IEA. Snapshot of Global PV Markets—2023 (2023).
- IEA. Clean Energy Market Monitor—March 2024 (2024).
- Chen, S. et al. Improved air quality in China can enhance solar-power performance and accelerate carbon-neutrality targets. *One Earth* **5**, 550–562 (2022).
- Zou, L. et al. Global surface solar radiation and photovoltaic power from Coupled Model Intercomparison Project Phase 5 climate models. *J. Clean. Prod.* **224**, 304–324 (2019).
- Gaetani, M. et al. The near future availability of photovoltaic energy in Europe and Africa in climate-aerosol modeling experiments. *Renew. Sustain. Energy Rev.* **38**, 706–716 (2014).
- AlSkaif, T., Dev, S., Visser, L., Hossari, M. & Van Sark, W. A systematic analysis of meteorological variables for PV output power estimation. *Renew. Energy* **153**, 12–22 (2020).
- Crook, J. A., Jones, L. A., Forster, P. M. & Crook, R. Climate change impacts on future photovoltaic and concentrated solar power energy output. *Energy Environ. Sci.* **4**, 3101–3109 (2011).
- Skoplaki, E. & Palyvos, J. A. On the temperature dependence of photovoltaic module electrical performance: a review of efficiency/power correlations. *Sol. Energy* **83**, 614–624 (2009).
- Li, L. et al. Mitigation of China's carbon neutrality to global warming. *Nat. Commun.* **13**, 5315 (2022).
- Chen, J., Cui, H., Xu, Y. & Ge, Q. Long-term temperature and sea-level rise stabilization before and beyond 2100: Estimating the additional climate mitigation contribution from China's recent 2060 carbon neutrality pledge. *Environ. Res. Lett.* **16**, 074032 (2021).
- Cheng, J. et al. A synergistic approach to air pollution control and carbon neutrality in China can avoid millions of premature deaths annually by 2060. *One Earth* **6**, 978–989 (2023).
- Liu, F. et al. Increased Asian aerosols drive a slowdown of Atlantic meridional overturning circulation. *Nat. Commun.* **15**, 18 (2024).
- Wang, P. et al. Aerosols overtake greenhouse gases causing a warmer climate and more weather extremes toward carbon neutrality. *Nat. Commun.* **14**, 7257 (2023).
- Yang, Y., Zeng, L., Wang, H., Wang, P. & Liao, H. Climate effects of future aerosol reductions for achieving carbon neutrality in China. *Sci. Bull.* **68**, 902–905 (2023).
- Liu, S. et al. Understanding of aerosol–climate interactions in China: aerosol impacts on solar radiation, temperature, cloud, and precipitation and its changes under future climate and emission scenarios. *Curr. Pollut. Rep.* **5**, 36–51 (2019).
- Zhang, J., You, Q. & Ullah, S. Changes in photovoltaic potential over China in a warmer future. *Environ. Res. Lett.* **17**, 114032 (2022).
- Feron, S., Cordero, R. R., Damiani, A. & Jackson, R. B. Climate change extremes and photovoltaic power output. *Nat. Sustain.* **4**, 270–276 (2020).
- Bichet, A. et al. Potential impact of climate change on solar resource in Africa for photovoltaic energy: analyses from CORDEX-AFRICA climate experiments. *Environ. Res. Lett.* **14**, 124039 (2019).
- Jerez, S. et al. The impact of climate change on photovoltaic power generation in Europe. *Nat. Commun.* **6**, 10014 (2015).
- Isaza, A., Kay, M., Evans, J. P., Prasad, A. & Bremner, S. Maximizing photovoltaic potential and minimizing costs in a future warmer climate: the role of atmospheric aerosols and greenhouse gas emissions. *Renew. Energy* **219**, 119561 (2023).
- Niu, J. et al. Climate change impact on photovoltaic power potential in China based on CMIP6 models. *Sci. Total Environ.* **858**, 159776 (2023).
- Lu, N. et al. High emission scenario substantially damages China's photovoltaic potential. *Geophys. Res. Lett.* **49**, e2022GL100068 (2022).
- Danso, D. K. et al. A CMIP6 assessment of the potential climate change impacts on solar photovoltaic energy and its atmospheric drivers in West Africa. *Environ. Res. Lett.* **17**, 044016 (2022).
- Hou, X., Wild, M., Folini, D., Kazadzis, S. & Wohland, J. Climate change impacts on solar power generation and its spatial variability in Europe based on CMIP6. *Earth Syst. Dyn.* **12**, 1099–1113 (2021).
- Zhang, D. et al. A representative CO<sub>2</sub> emissions pathway for China toward carbon neutrality under the Paris Agreement's 2 °C target. *Adv. Clim. Chang. Res.* **14**, 941–951 (2023).
- Cheng, J. et al. Comparison of current and future PM<sub>2.5</sub> air quality in China under CMIP6 and DPEC emission scenarios. *Geophys. Res. Lett.* **48**, e2021GL093197 (2021).
- Wang, Z. et al. Incorrect Asian aerosols affecting the attribution and projection of regional climate change in CMIP6 models. *npj Clim. Atmos. Sci.* **4**, 2 (2021).
- Qin, Y. et al. Amplified positive effects on air quality, health, and renewable energy under China's carbon-neutral target. *Nat. Geosci.* **17**, 411–418 (2024).
- Ren, L. et al. Co-benefits of mitigating aerosol pollution to future solar and wind energy in China toward carbon neutrality. *Geophys. Res. Lett.* **51**, e2024GL109296 (2024).
- Zheng, D. et al. Climate change impacts on the extreme power shortage events of wind-solar supply systems worldwide during 1980–2022. *Nat. Commun.* **15**, 5225 (2024).
- Lei, Y. et al. Co-benefits of carbon neutrality in enhancing and stabilizing solar and wind energy. *Nat. Clim. Chang.* **13**, 693–700 (2023).
- Jacobson, M. Z. & Jadhav, V. World estimates of PV optimal tilt angles and ratios of sunlight incident upon tilted and tracked PV panels relative to horizontal panels. *Sol. Energy* **169**, 55–66 (2018).
- Wang, Z. et al. Evaluation of surface solar radiation trends over China since the 1960s in the CMIP6 models and potential impact of aerosol emissions. *Atmos. Res.* **268**, 105991 (2022).
- Huang, G. et al. Critical climate issues toward carbon neutrality targets. *Fundam. Res.* **2**, 396–400 (2022).
- Danabasoglu, G. et al. The Community Earth System Model Version 2 (CESM2). *J. Adv. Model. Earth Syst.* **12**, e2019MS001916 (2020).
- Fricko, O. et al. The marker quantification of the Shared Socioeconomic Pathway 2: a middle-of-the-road scenario for the 21st century. *Glob. Environ. Change* **42**, 251–267 (2017).
- O'Neill, B. C. et al. The Scenario Model Intercomparison Project (ScenarioMIP) for CMIP6. *Geosci. Model Dev.* **9**, 3461–3482 (2016).
- Strandsbjerg, J. et al. An assessment of the performance of scenarios against historical global emissions for IPCC reports. *Glob. Environ. Change* **66**, 102199 (2021).

45. Cannon, A. J. Multivariate quantile mapping bias correction: an N-dimensional probability density function transform for climate model simulations of multiple variables. *Clim. Dyn.* **50**, 31–49 (2018).
46. Cannon, A. J., Sobie, S. R. & Murdock, T. Q. Bias correction of GCM precipitation by quantile mapping: how well do methods preserve changes in quantiles and extremes? *J. Clim.* **28**, 6938–6959 (2015).
47. Li, Y.-F. et al. Sorely reducing emissions of non-methane short-lived climate forcers will worsen compound flood-heatwave extremes in the Northern Hemisphere. *Adv. Clim. Chang. Res.* **15**, 737–750 (2024).
48. Xu, Z., Han, Y., Tam, C.-Y., Yang, Z.-L. & Fu, C. Bias-corrected CMIP6 global dataset for dynamical downscaling of the historical and future climate (1979–2100). *Sci. Data* **8**, 293 (2021).
49. Lei, Y. et al. Global solar droughts due to supply-demand imbalance exacerbated by anthropogenic climate change. *Geophys. Res. Lett.* **51**, e2024GL112162 (2024).
50. Park, C. et al. What determines future changes in photovoltaic potential over East Asia? *Renew. Energy* **185**, 338–347 (2022).
51. Perkins, S. E. & Alexander, L. V. On the measurement of heat waves. *J. Clim.* **26**, 4500–4517 (2013).

### Acknowledgements

This work was jointly supported by the Special Project of the National Natural Science Foundation of China (42341202), the National Natural Science Foundation of China (42275042), the Science and Technology Development Fund of CAMS (2024KJ004), and the National Key Scientific and Technological Infrastructure project “Earth System Numerical Simulation Facility” (EarthLab). We acknowledge the MEIC team for developing and providing the anthropogenic emission inventories of China.

### Author contributions

Z.L.W. and Y.D.L. designed the research and defined the framework for this study. Z.Y.H. and Z.G. conducted the model simulations. Z.Y.H. processed the data and performed the analysis with substantial contributions from Z.L.W., Y.D.L., X.C.Y., and Y.F.L. Z.Y.H., Z.L.W., Y.D.L., and X.C.Y. led the paper writing with substantial contributions from all co-authors.

### Competing interests

The authors declare no competing interests.

### Additional information

**Supplementary information** The online version contains supplementary material available at <https://doi.org/10.1038/s41612-025-01005-z>.

**Correspondence** and requests for materials should be addressed to Zhili Wang or Yadong Lei.

**Reprints and permissions information** is available at <http://www.nature.com/reprints>

**Publisher’s note** Springer Nature remains neutral with regard to jurisdictional claims in published maps and institutional affiliations.

**Open Access** This article is licensed under a Creative Commons Attribution-NonCommercial-NoDerivatives 4.0 International License, which permits any non-commercial use, sharing, distribution and reproduction in any medium or format, as long as you give appropriate credit to the original author(s) and the source, provide a link to the Creative Commons licence, and indicate if you modified the licensed material. You do not have permission under this licence to share adapted material derived from this article or parts of it. The images or other third party material in this article are included in the article’s Creative Commons licence, unless indicated otherwise in a credit line to the material. If material is not included in the article’s Creative Commons licence and your intended use is not permitted by statutory regulation or exceeds the permitted use, you will need to obtain permission directly from the copyright holder. To view a copy of this licence, visit <http://creativecommons.org/licenses/by-nc-nd/4.0/>.

© The Author(s) 2025